NASA/TM—2000-210518 AIAA–2000–3814

Performance of Titanium Optics on a NASA 30 cm Ion Thruster

George C. Soulas, John E. Foster, and Michael J. Patterson
Glenn Research Center, Cleveland, Ohio

November 2000

The NASA STI Program Office . . . in Profile

Since its founding, NASA has been dedicated to the advancement of aeronautics and space science. The NASA Scientific and Technical Information (STI) Program Office plays a key part in helping NASA maintain this important role.

The NASA STI Program Office is operated by Langley Research Center, the Lead Center for NASA's scientific and technical information. The NASA STI Program Office provides access to the NASA STI Database, the largest collection of aeronautical and space science STI in the world. The Program Office is also NASA's institutional mechanism for disseminating the results of its research and development activities. These results are published by NASA in the NASA STI Report Series, which includes the following report types:

- TECHNICAL PUBLICATION. Reports of completed research or a major significant phase of research that present the results of NASA programs and include extensive data or theoretical analysis. Includes compilations of significant scientific and technical data and information deemed to be of continuing reference value. NASA's counterpart of peer-reviewed formal professional papers but has less stringent limitations on manuscript length and extent of graphic presentations.

- TECHNICAL MEMORANDUM. Scientific and technical findings that are preliminary or of specialized interest, e.g., quick release reports, working papers, and bibliographies that contain minimal annotation. Does not contain extensive analysis.

- CONTRACTOR REPORT. Scientific and technical findings by NASA-sponsored contractors and grantees.

- CONFERENCE PUBLICATION. Collected papers from scientific and technical conferences, symposia, seminars, or other meetings sponsored or cosponsored by NASA.

- SPECIAL PUBLICATION. Scientific, technical, or historical information from NASA programs, projects, and missions, often concerned with subjects having substantial public interest.

- TECHNICAL TRANSLATION. English-language translations of foreign scientific and technical material pertinent to NASA's mission.

Specialized services that complement the STI Program Office's diverse offerings include creating custom thesauri, building customized data bases, organizing and publishing research results . . . even providing videos.

For more information about the NASA STI Program Office, see the following:

- Access the NASA STI Program Home Page at ***http://www.sti.nasa.gov***

- E-mail your question via the Internet to help@sti.nasa.gov

- Fax your question to the NASA Access Help Desk at 301–621-0134

- Telephone the NASA Access Help Desk at 301–621–0390

- Write to:
  NASA Access Help Desk
  NASA Center for AeroSpace Information
  7121 Standard Drive
  Hanover, MD 21076

NASA/TM—2000-210518 AIAA–2000–3814

Performance of Titanium Optics on a NASA 30 cm Ion Thruster

George C. Soulas, John E. Foster, and Michael J. Patterson
Glenn Research Center, Cleveland, Ohio

Prepared for the
36th Joint Propulsion Conference and Exhibit
cosponsored by the AIAA, ASME, SAE, and ASEE
Huntsville, Alabama, July 17–19, 2000

National Aeronautics and
Space Administration

Glenn Research Center

November 2000

This report contains preliminary findings, subject to revision as analysis proceeds.

Available from

NASA Center for Aerospace Information
7121 Standard Drive
Hanover, MD 21076
Price Code: A03

National Technical Information Service
5285 Port Royal Road
Springfield, VA 22100
Price Code: A03

Available electronically at http://gltrs.grc.nasa.gov/GLTRS

PERFORMANCE OF TITANIUM OPTICS ON A NASA 30 CM ION THRUSTER

George C. Soulas, John E. Foster, and Michael J. Patterson
National Aeronautics and Space Administration
Glenn Research Center
Cleveland, Ohio 44135

The results of performance tests with two titanium optics sets are presented and compared to those of molybdenum optics. All tests were conducted on a 30 cm ion thruster that was nearly identical to the NSTAR thruster design. Optics performance tests were conducted over a thruster input power range of 0.5 to 4.6 kW. Optics performance including impingement-limited total voltages, electron backstreaming limits, screen grid ion transparencies, near-field beam current density profiles, beam divergence angles, and beam divergence thrust correction factors were determined throughout this power range. The impingement-limited total voltages for titanium optics were within 10-55 V of those for molybdenum optics. Electron backstreaming limit magnitude as a function of peak beam current density for both molybdenum and titanium optics were within a few volts of each other, indicating similar hot grid gaps for these two grid materials during steady-state operation. Beam divergence half-angles at 90% of the total beam current and thrust correction factors for both titanium optics sets were within 1° and 1%, respectively, of those for molybdenum optics. When thruster power was increased to 2.3 kW immediately following discharge ignition, the titanium screen grid came into contact with the accelerator grid within 5 minutes of ignition. Relative to molybdenum, titanium's larger thermal expansion and smaller thermal conductivity likely caused the screen grid to thermally expand more relative to the accelerator grid during startup.

Introduction

The success of the NSTAR (i.e., NASA Solar Electric Propulsion Technology Applications Readiness Program) 30 cm ion thruster system on the Deep Space 1 mission has demonstrated the viability of ion propulsion for deep space missions.[1,2] As a result, ion propulsion is being considered for several deep space missions, such as the Comet Nucleus Sample Return, Venus Sample Return, Saturn Ring Observer, Neptune Orbiter, Titan Explorer, and others. However, most of these missions require increasing the NSTAR thruster's propellant throughput and peak input power capabilities beyond the demonstrated 88 kg of xenon at 2.3 kW.[3]

Increasing propellant throughput and thruster power is limited, in part, by charge-exchange sputter erosion of the accelerator grid.[3,4] Significant charge-exchange accelerator grid sputter erosion can lead to three likely failure mechanisms:[5]

1. electron backstreaming due to accelerator aperture enlargement;
2. structural failure of the grid due to pit and groove erosion of the downstream accelerator surface; and
3. an unclearable grid short by a flake from sputter-eroded accelerator grid material.

Changing the ion optics material to one with a lower volumetric sputter erosion rate addresses all of the aforementioned failure mechanisms to extend propellant throughput and thruster power density.

A development effort was, therefore, initiated at the NASA Glenn Research Center (GRC) to identify a material with a lower accelerator grid volumetric sputter erosion rate than molybdenum, but that could utilize the present NSTAR thruster grid design and fabrication techniques to keep development costs low, and perform as well as molybdenum optics.[6] Titanium was found to offer a 45% reduction in volumetric erosion rates and could be fabricated using the same fabrication techniques as molybdenum optics. Accelerator grid life was expected to be improved by a factor of 1.9x. Analyses of fabrication, launch environment, and thruster operation with titanium revealed no significant issues. Several titanium grid sets were successfully fabricated. A titanium optics set was mounted onto an NSTAR 30 cm engineering model ion thruster and tested to determine optics performance. The titanium optics operated successfully over the entire NSTAR power range of 0.5 to 2.3 kW. Differences in impingement-limited total voltages (or perveance) and electron backstreaming limits were speculated to be due to a larger cold gap for the titanium optics. Discharge losses for titanium grids were lower than those for molybdenum, likely due to a larger titanium screen grid open area fraction. Radial

distributions of beam current density with titanium optics were very similar to those with molybdenum optics at all power levels.

Because the large cold gap of the prior titanium optics tests prevented a one-to-one comparison with molybdenum optics, additional optics performance tests were conducted. This paper reports on the results of these tests. Included are performance tests of the 30 cm titanium optics of ref. 6 which were re-gapped to improve perveance, and an unused titanium optics set. Optics performance tests were conducted over a broader thruster input power range of 0.5 to 4.6 kW and compared to those of molybdenum optics using the same thruster. Optics performance parameters such as impingement-limited total voltages, electron backstreaming limits, screen grid ion transparencies, near-field beam current density profiles, beam divergence angles, and beam divergence thrust correction factors were determined throughout the thruster input power range.

Test Hardware and Operating Procedures

Titanium Optics

A photograph of 30 cm titanium grids is shown in Fig. 1. Two titanium optics sets are reported in this paper. The first set, identified as set A, was the same as that reported in ref. 6 and had accumulated about 11 hours of operation with beam extraction prior to these tests. In that earlier report, the grid cold gap along the outer perimeter of the active area was set to that of the NSTAR design,[7,8] while the cold gap at the active area mid-radius and center was measured to be about 23-38% larger. For the tests reported in this paper, the grid cold gap at the active area mid-radius and center was set to that of the NSTAR design. It was anticipated that decreasing the cold gap at the active area mid-radius and center to the nominal design gap would aid in improving perveance since the beam current density is highest in these regions. The resulting cold gap at the active area outer perimeter was 23-27% smaller than the NSTAR design. Screen grid aperture diameters were 7% larger than the nominal design at the active area mid-radius and center while accelerator aperture diameters were within ±11% of the nominal design. These variations from the nominal design were not intentional, but were a result of the chemical etching process used to create the grid apertures. The magnitudes of these variations decreased as the manufacturer gained experience fabricating titanium optics.[6] Aperture diameter variations for molybdenum screen and accelerator grids are typically within ±2.7% and ±4.4%, respectively, of the nominal NSTAR design dimensions.

The second titanium grid set, identified as set B, had not been operated prior to these tests. Screen and accelerator grid aperture diameter variations were within ±2% and ±9%, respectively, of the nominal NSTAR design at the active area mid-radius and center. Grid cold gap variations throughout the active area were within ±4% of the nominal NSTAR design, which was better than the ±8% variations for the molybdenum optics used for these tests. The uniformity of the cold gap for set B versus that for set A may have been due to the different mechanical properties of the accelerator grid material lot used for grid set B.

Molybdenum Optics

Molybdenum optics fabricated at NASA GRC were also tested to provide a baseline performance for comparison. The molybdenum optics utilized the NSTAR optics geometry, which is described in refs. 7 and 8, and had accumulated about 20 hours of operation with beam extraction prior to these tests.

Ion Thruster

The optics sets were mounted onto a 30 cm ion thruster, which is shown in Fig. 2. This thruster serves as a test bed for 5 kW thruster development at NASA.[9] The thruster mechanical design is nearly identical to that of the NSTAR thruster, described in detail in refs. 7 and 8, with the only significant difference being the materials used for the discharge chamber. The thruster was fitted with thermocouples for thermal tests and plasma diagnostics for discharge chamber plasma investigations,[10] and the exterior was modified so that a second neutralizer could be installed for separate neutralizer tests.[9]

Power Console and Gas Feed System

A power console similar to that described in ref. 11 powered the thruster. This power console was modified to allow the thruster to be throttled up to 5 kW. A high purity gas feed system was used to provide xenon to the discharge cathode, discharge chamber, and neutralizer through separate mass flow controllers.

Diagnostics

During thruster operation, voltages and currents were measured with digital multimeters and xenon flows with mass flow meters. These measured parameters were used to set thruster operating conditions, as well as to determine thruster performance.

The thruster was connected to an electrically floating power supply circuit used to determine the screen grid transparency to discharge chamber ions. The circuit electrically tied the screen grid to the discharge cathode during normal operation, but biased the grid negative relative to discharge cathode potential to repel electrons and measure the collected ion current.

Beam current density profiles were measured with a Faraday probe mounted onto a two-axis probe motion

system. The Faraday probe was a planar geometry with a 1.0 cm^2 circular current-collecting area.[10] The probe was biased negative with respect to beam plasma potential to repel electrons and was grounded through a resistor that acted as a shunt to measure collected currents.

The positioning system swept the Faraday probe in the radial and axial directions through the vertical center of the thruster optics. The positioning system had a 1.25 m maximum travel in each axis, which enabled near-field radial beam current density measurements at different axial locations as measured from the geometric center of the optics. The current density measurements were then used to determine beam current density profiles, beam divergence half-angles, and thrust correction factors.

Vacuum Facility

Testing was conducted in Vacuum Facility 11 at NASA GRC. The facility is 2.2 m in diameter and 7.9 m in length. Seven cryogenic pumps and a turbomolecular pump evacuated the facility. The total measured pumping speed of the facility was 110,000 l/s with xenon. The facility base pressure was typically 1.3×10^{-5} Pa (1×10^{-7} Torr) and background pressures were as high as 6.6×10^{-4} Pa (4.9×10^{-6} Torr) at the peak thruster input power of 4.6 kW.

Operating Procedures

Molybdenum and titanium optics were performance tested on the 30 cm ion thruster. During each test, the thruster was typically step-ramped through the nominal NSTAR thruster input power levels of 2.3, 1.8, 1.7, 1.4, 1.0, and 0.5 kW, which corresponded to nominal thruster voltages, currents, and xenon flows listed in Table 1 (a complete listing of NSTAR power levels can be found in ref. 12). In addition, the thruster was also operated at 3.0 kW and 4.6 kW, with corresponding operating parameters also listed in Table 1. At each power level, optics performance parameters such as impingement-limited total voltages, electron backstreaming limits, screen grid ion transparencies, and beam current density profiles, as well as other thruster performance parameters, were determined.

Results and Discussions

Molybdenum optics were first tested on the 30 cm ion thruster to obtain a baseline performance for comparison to titanium optics. Titanium optics sets A and B were then tested. During one test for titanium optics set B, the thruster was started from room temperature and increased to 2.3 kW immediately following discharge ignition to monitor thermal effects on the grid gap. All optics sets operated successfully over the entire 0.5 to 4.6 kW power range. The following sections will present and discuss the results of these tests.

Impingement-Limited Total Voltage

Impingement-limited total voltage is a measure of optics' current extraction capability, and, therefore, a measure of optics perveance. Impingement-limited total voltages were determined from plots of accelerator current as a function of total voltage where the slope was -0.02 mA/V. Perveance margins were defined as the difference between the total voltage during normal operation (i.e. the settings defined in Table 1) and the impingement-limited total voltage. Beam current as a function of impingement-limited total voltage is plotted in Fig. 3 for titanium and molybdenum optics. Perveance margins for both titanium optics sets are listed in Table 2 with results from molybdenum optics for comparison.

As Fig. 3 and Table 2 demonstrate, impingement-limited total voltages decreased by 30-65 V for titanium optics set A when the cold gap at the active area mid-radius and center was decreased to the nominal NSTAR gap. The improved impingement-limited total voltages of titanium optics set A, however, were still 40-125 V higher than those of molybdenum optics. This difference is likely due, in large part, to the 7% larger screen grid aperture diameters for set A. The larger screen grid aperture diameters resulted in a smaller accelerator-to-screen aperture diameter ratio, which is known to increase impingement-limited total voltage.[13]

Impingement-limited total voltages for titanium optics set B were only 10-55 V higher than those of molybdenum. This agreement is considered sufficient, especially because impingement-limited total voltages are known to decrease with thruster operation.[3]

Titanium optics set B was initially tested at an input power range of 0.5 to 4.6 kW, and then 1.0 to 2.3 kW. Impingement-limited total voltages decreased by 45-50 V by the second test. Since beam current density profiles did not change significantly during these tests, there are only two parameters that could have improved optics perveance for a given thruster operating condition: 1) a decrease in the grid hot gap, or 2) an increase of accelerator aperture diameter. It is unlikely that the hot grid gap changed during testing since a post-test examination showed no measurable change in the grid cold gap. It is, therefore, speculated that the rapid perveance limit improvement was due to an initial enlargement of the accelerator grid apertures through sputter-erosion. This increased sputter erosion may have been due to slight aperture misalignments that allowed beam ions to impinge the accelerator grid. Similar rapid improvements in perveance have also been reported with molybdenum optics.[14] These perveance improvements were not noted with titanium

optics set A nor with the molybdenum optics since each had accumulated 10-20 hours of operation prior to these performance tests. Only the results from the second test of titanium optics set B (i.e. 1.0 to 2.3 kW) are presented in this paper since the optics had accumulated about 15 hours of operation by the start of that test.

Electron Backstreaming Limit

The NSTAR ion thruster operates at high net-to-total accelerating voltages in order to minimize accelerator grid erosion. As a result, the electron backstreaming limit voltages of titanium optics should be similar to those of molybdenum optics in order to take full advantage of the reduced volumetric sputter erosion offered by titanium. The electron backstreaming limit was determined by lowering the magnitude of the accelerator grid voltage until the indicated beam current increased by 0.1 mA due to backstreaming electrons. Electron backstreaming limit voltages for the titanium optics are listed in Table 2 with results with molybdenum optics for comparison.

Table 2 shows that the decreased cold gap for titanium optics set A increased the electron backstreaming limit magnitudes, as was expected. This is demonstrated by the semi-empirical equation derived by Kaufman to solve for the magnitude of the electron backstreaming limit voltage: [15]

$$(1-R_{max}) = \frac{|V_{eb}|}{V_{b\text{-}PS} + |V_{eb}|} = \frac{0.2}{\frac{l_e}{d_a} \cdot \exp\left(\frac{t_a}{d_a}\right)}. \quad (1)$$

Here, R_{max} is the maximum net-to-total accelerating voltage, V_{eb} is the electron backstreaming limit, $V_{b\text{-}PS}$ is the beam power supply voltage, d_a is the accelerator aperture diameter, t_a is the accelerator grid thickness, and l_e is the effective acceleration length. The effective acceleration length is given by: [16]

$$l_e = \sqrt{(l_g + t_s)^2 + \left(\frac{d_s}{2}\right)^2}, \quad (2)$$

where t_s is the screen grid thickness and l_g is the hot gap, which will be assumed to be the cold gap. The increased electron backstreaming limits for set A were 2-5 V greater than those of the molybdenum optics. However, titanium optics set A had a larger peak beam current density than the molybdenum optics (discussed later). Since the electron backstreaming limit is also a function of the peak beam current density,[17] the electron backstreaming limit is plotted as a function of the peak beam current density (listed in Table 3) in Fig. 4 for a more appropriate comparison. The data for each grid set are presented at separate beam voltages because the electron backstreaming limit is also a function of beam voltage, as shown in equation 1. As the figure shows, the electron backstreaming limit magnitude as a function of peak beam current density for the molybdenum optics was about 3 V greater than that of titanium optics set A at a beam power supply voltage of 1100 V. This was expected since the effective acceleration length for titanium optics set A was about 4% larger than that of the molybdenum optics due to the larger screen aperture diameters for set A (see equation 2).

Table 2 and Fig. 4 show that the electron backstreaming limit magnitudes for titanium optics set B were within 4 V of those for titanium optics set A. As Fig. 4 further shows, the electron backstreaming limit magnitude as a function of peak beam current density for the molybdenum optics was about 2-3 V greater than that of titanium optics set B at a beam power supply voltage of 1100 V.

Because the electron backstreaming limit magnitudes as a function of peak beam current density for both molybdenum and titanium optics were within a few volts, the difference in hot gap for these two grid materials is likely insignificant during steady-state operation. This is noteworthy since titanium has a 1.8x larger thermal expansion than molybdenum.[6]

Screen Grid Ion Transparency

Screen grid ion transparency is a function of screen grid geometry and, therefore, can give insight to geometric differences between grid sets. Table 3 lists screen grid ion transparencies for titanium optics with results from molybdenum optics for comparison. Screen grid ion transparencies were calculated with the following equation:

$$\phi = \frac{J_b}{J_{b,bias} + J_{s,bias}}, \quad (3)$$

where φ is the screen grid ion transparency, J_b is the beam current, $J_{b,bias}$ is the beam current when the screen grid is biased, and $J_{s,bias}$ is the current collected to the screen grid when it is biased. The numerator denotes the extracted ion current while the denominator denotes the total ion current arriving at the screen grid. The beam current with screen grid bias is used in the denominator because it always decreased by less than 2.2% when the screen grid was biased negative. This is because the potential difference between the screen grid and the discharge plasma was increased when the screen grid was biased, and this increase caused the sheath to direct ions into the webbing.[18]

Screen grid ion transparencies reflected the similar screen grid open area fractions for titanium optics set B and the molybdenum optics. In contrast, ion transparencies for titanium optics set A were 5-7% greater than those for the molybdenum optics, reflecting the larger physical open area fraction for titanium optics set A at the active area mid-radius and center.

Beam Current Density Profiles, Beam Divergence, and Thrust Losses

Beam current density profiles were used to determine beam divergence and thrust loss, and to provide peak values for comparisons of electron backstreaming limits. Regarding beam current density measurements, no attempt was made to repel charge-exchange ions from the Faraday probe or to account for secondary electron emission due to ion bombardment. Errors due to secondary electron emission from singly-charge beam ions are anticipated to be only 1.5%.[19] Integration of the radial beam current density profiles (assuming azimuthal symmetry) yielded beam currents that were higher than the measured beam current by as much as 15%. It is anticipated that this error was caused by a combination of effects, which included the large probe surface area, measurement of charge-exchange ions in the beam, and secondary electron emission from both singly- and doubly-charged ions.

Peak beam current densities were determined from radial beam current density profiles taken 49 mm downstream of the grid center. Sample radial beam current density distributions are shown in Fig. 5. Table 3 lists peak beam current densities for titanium optics with results from molybdenum optics for comparison. As Table 3 shows, peak beam current densities for both titanium optics sets A and B were 13-16% higher than those for molybdenum optics. However, electron backstreaming limits as a function of peak beam current densities showed no significant differences in optics geometry between titanium optics set B and the molybdenum optics. It is presently unclear whether this change in peak beam current density was due to the optics or some change in the thruster discharge chamber.

Figure 5 also shows that all beam current density profiles were slightly non-axisymmetric near the active area center. Furthermore, this slight asymmetry occurred for all power levels tested. This asymmetry is an artifact of the thruster discharge chamber plasma and has been noticed in other NSTAR thrusters.[3]

Beam divergence half-angles were determined in the following manner. Beam current density profiles were taken at five axial locations, examples of which are shown in Fig. 6. At each axial location, the fraction of total integrated beam current as a function of radius was determined by:

$$f(r,z)=\frac{\int_0^r j_b(r,z)\cdot r\cdot dr}{\int_0^\infty j_b(r,z)\cdot r\cdot dr}. \qquad (4)$$

Here, f is the fraction of the total integrated beam current, j_b is the beam current density, r is the radial location, and z is the axial location. Note that azimuthal symmetry is assumed in equation 4. Although beam current density profiles were found to be slightly non-axisymmetric near the grid center, this asymmetry accounted for only 10-20% of the total beam current. To ensure that results were conservative, however, the radial side opposite the peak beam current density (i.e. the positive radii in Fig. 5) was used in these calculations.

Sample total beam current fractions are shown in Fig. 7. Since these fractions were linear, linear regression could be used to determine slope of each fraction. The divergence half-angle could then be determined using the following equation:

$$\beta_f = \arctan\left(\frac{1}{s_f}\right), \qquad (5)$$

where β_f and s_f were the divergence half-angle and slope, respectively, for a given total beam current fraction. From these values, plots of percentage of total beam current as a function of divergence half-angle were generated, samples of which are shown in Fig. 8.

Beam divergence angles at 90% of the total beam current are listed in Table 4 for titanium optics set A with results from molybdenum optics for comparison. Divergence half-angle data for titanium optics sets A and B were within 1° of those for molybdenum optics. Fig. 8 also compares beam current percentages as a function of divergence half-angle at 2.3 kW for titanium and molybdenum optics. Beam divergence half-angles were almost identical for both optics materials.

The beam divergence half-angle data can further be used to determine the thrust correction factor for beam divergence. Ion engine thrust, T, is given by:

$$T = \alpha_t \cdot F_t \cdot J_b \cdot \sqrt{\frac{2\cdot m_i \cdot V_b}{e}}, \qquad (6)$$

where α_t and F_t are the thrust correction factors for doubly-charged ions and beam divergence, respectively, J_b and V_b are the beam current and voltage, respectively, m_i is the ion mass, and e is the electronic charge. The correction factor for doubly-charged ions is given by:

$$\alpha_t = \frac{1+\frac{J^{++}}{J^+}\cdot\frac{1}{\sqrt{2}}}{1+\frac{J^{++}}{J^+}}, \qquad (7)$$

where J^{++}/J^+ is the ratio of double-to-single ion current. The thrust correction factor for beam divergence is given by:

$$F_t = \frac{\int_0^{2\pi}\int_0^{\infty} j_b \cdot \cos(\beta) \cdot r \cdot dr \cdot d\theta}{\int_0^{2\pi}\int_0^{\infty} j_b \cdot r \cdot dr \cdot d\theta} . \quad (8)$$

Two assumptions are made for equations 6-8: 1) the ratio of double-to-single beam current density is constant throughout the active area; and 2) the divergence half-angle for doubly-charged ions is the same as those for singly-charged ions. If azimuthal symmetry is assumed, the measured beam divergence half-angle results can be used to determine this correction factor (i.e. equation 8). As mentioned previously, because the beam current density profile was the slightly non-axisymmetric, the radial side opposite the peak beam current density was used in these calculations to ensure that results were conservative.

Table 4 lists these thrust correction factors for titanium optics set A with results from molybdenum optics for comparison. All values for titanium optics set A were within 1% of those with molybdenum optics. This close agreement demonstrates that thrust losses from beam divergence are very similar for titanium and molybdenum optics. It is noteworthy that the thrust correction factors in Table 4 are within about 1% of 0.98 thrust correction factor predicted by Patterson, Haag, and Hovan.[20]

Thermally-Induced Effects During Thruster Startup

The aforementioned test results were obtained with the optics thermally at or near steady state. As a result, the hot gap between the screen and accelerator grids was stable. This was intermittently confirmed during testing by ensuring that the electron backstreaming limit, which is a function of grid gap (see equations 1 and 2), had stabilized to within 2-3 V. During thruster startup, however, thermal transients and uneven heating of the screen and accelerator grids causes the grid gap to significantly decrease, then increase to a stable value. MacRae, Zavesky, and Gooder reported on the measured temporal changes in grid gap during thruster startup for three 30 cm molybdenum optics assemblies that were predecessors to the NSTAR design.[21] At discharge powers comparable to 2.3 kW thruster operation, they found that the grid gap decreased by as much as 62% of the cold gap, and that these minimum gaps occurred within about 4 minutes of discharge ignition. Grid gaps increased thereafter, and were within 5% of the cold gap within 16 minutes of discharge ignition.

As a final test for titanium optics set B, the thruster was started from room temperature and operated with beam extraction within 1 minute of discharge ignition. The objective was to use temporal electron backstreaming limit changes to gain insight into grid gap changes as was done in ref. 6. The thruster was increased to about 2.3 kW within 1.3 minutes of discharge ignition. Operating conditions were the same as those listed in Table 1 for 2.3 kW, except that the accelerator voltage was set to –320 V to prevent electron backstreaming during startup. At 4.6 minutes, the screen grid came into contact with the accelerator grid. During one of the several recycles that resulted from this contact, enough energy was provided to this region of contact for the grids to bond together.

A post-test inspection of set B revealed that the grids bonded in an approximately 4-5 mm diameter circular region that appeared to coincide with the peak beam current density. This bonded region further coincided with the white spot near the center of the optics in Fig. 2. Only the screen grid dome appeared deformed, likely because of its larger open area fraction and smaller thickness relative to the accelerator grid. A grid-gapping gage was used to successfully separate the grids. Following separation, aperture alignment and grid cold gap were checked and changes were found to be negligible. This indicates that the screen grid returned to its original shape, which is not surprising given titanium's low elastic modulus and high yield strength.[6]

Titanium's thermal expansion and thermal conductivity are 1.8x and 0.12x those of molybdenum, respectively.[6] These material properties likely caused the titanium screen grid to expand more relative to the accelerator grid under thermal loads. Although electrostatic pressure increased as the grids neared each other, electrostatic pressure was likely insignificant since the pressure required to move the screen grid the remainder of the distance just prior to contact was calculated to be less than 1% of the initial cold gap. It is doubtful that the optics could have sustained such a high voltage over such a small distance without first arcing. That there was enough power provided by the beam and accelerator power supplies to bond the grids is likely a material property, but is still being investigated. This grid-to-grid contact was not noticed in ref. 6 and may have been avoided by the larger cold gap in the active area mid-radius and center for that titanium optics set. It is noteworthy that the titanium optics made contact in almost the same time that it took for the molybdenum optics in ref. 21 to reach their minimum hot gap at similar operating conditions. There is no known record of domed molybdenum optics bonding to each other as a result of thruster operation at NASA or Hughes Space and Communications Company.[22, 23]

An obvious method of precluding grid-to-grid bonding would be to allow the discharge chamber plasma to heat the optics for some period prior to beam extraction. A method of preventing grid-to-grid contact

would be to ignite the discharge at the lowest power level and throttle it up to the desired operating point slower than would be done for molybdenum optics. Data from MacRae, Zavesky, and Gooder show that lower discharge powers typically resulted in larger hot grid gap minima following thruster startup.[21]

Conclusions

The results of performance tests with titanium optics were presented. Titanium optics sets included those of ref. 6, identified as set A, which were re-gapped to improve perveance and an unused set identified as set B. Molybdenum optics were also tested to provide a baseline performance for comparison. All tests were conducted with a 30 cm ion thruster that was nearly identical in mechanical design to that of the NSTAR thruster. Thruster diagnostics included an electrically floating power supply circuit to determine the screen grid ion transparency and a Faraday probe mounted onto a two-axis probe motion system to measure beam current density profiles.

Impingement-limited total voltages decreased by 30-65 V for titanium optics set A when the cold gap at the active area mid-radius and center was decreased to the nominal NSTAR gap. Impingement-limited total voltages for titanium optics set B were only 10-55 V higher than those of molybdenum. This agreement is considered sufficient, especially since impingement-limited total voltages are known to decrease with thruster operation. Titanium optics set B also exhibited an initial rapid perveance improvement that was thought to be due to an initial enlargement of the accelerator grid apertures through sputter-erosion.

Electron backstreaming limit magnitudes as a function of peak beam current density for both molybdenum and titanium optics were within a few volts of each other. This indicates that the difference in hot gap for these two optics materials was likely insignificant during steady-state operation.

Screen grid ion transparencies reflected the similar screen grid open area fractions for titanium optics set B and the molybdenum optics. In contrast, ion transparencies for titanium optics set A were 5-7% greater than those for the molybdenum optics, reflecting the larger open area fraction for titanium optics set A at the active area mid-radius and center.

Beam divergence half-angles at 90% of the total beam current for titanium optics sets A were within 1° of those for molybdenum optics. All beam divergence thrust correction factors for both titanium optics sets were within 1% of those with molybdenum optics.

When the thruster was set to 2.3 kW immediately following discharge ignition, the screen grid of titanium optics set B came into contact with the accelerator grid within 5 minutes of ignition. Relative to molybdenum, titanium's larger thermal expansion and smaller thermal conductivity likely caused the screen grid to thermally expand more relative to the accelerator grid during thruster startup.

References

[1] Rawlin, V.K., et al. "An Ion Propulsion System for NASA's Deep Space Missions," AIAA Paper 99-4612, September 1999.

[2] Polk, J.E., et al., "Validation of the NSTAR Ion Propulsion System on Deep Space One Mission: Overview and Initial Results," AIAA Paper 99-2274, June 1999.

[3] Polk, J.E., et al., "An Overview of the Results from an 8200 Hour Wear Test of the NSTAR Ion Thruster," AIAA Paper 99-2446, June 1999.

[4] Rawlin, V.K., "Erosion Characteristics of Two-Grid Ion Accelerating Systems," IEPC Paper 93-175, September 1993.

[5] Brophy, J.R., Polk, J.E., and Rawlin, V.K., "Ion Engine Service Life Validation by Analysis and Testing," AIAA Paper 96-2715, July 1996.

[6] Soulas, G.C., Haag, T.W., Patterson, M.J., and Rawlin, V.K., "Titanium Optics for Ion Thrusters," IEPC Paper 99-149, October 1999.

[7] Christensen, J.A., et al., "Design and Fabrication of a Flight Model 2.3 kW Ion Thruster for the Deep Space 1 Mission," AIAA Paper 98-3327, July 1998.

[8] Sovey, J.S., et al., "Development of an Ion Thruster and Power Processor for New Millennium's Deep Space 1 Mission," AIAA Paper 97-2778, December 1997.

[9] Patterson, M.J., et al., "Ion Propulsion Development Activities at NASA Glenn Research Center," AIAA Paper 2000-3810, July 2000.

[10] Foster, J.E., Soulas, G.C., and Patterson, M.J., "Plume and Discharge Plasma Measurements of a 5 kW NSTAR-Derivative Ion Thruster," AIAA Paper 2000-3812, July 2000.

[11] Pinero, L.R., Patterson, M.J., and Satterwhite, V.E., "Power Console Development for NASA's Electric Propulsion Outreach Program," IEPC Paper 93-250, September 1993.

[12] Rawlin, V.K., et al., "NSTAR Flight Thruster Qualification Testing," AIAA Paper 98-3936, July 1998.

[13] Rovang, D.C. and Wilbur, P.J., "Ion Extraction Capabilities of Two-Grid Accelerator Systems," IEPC Paper 84-86, July 1984.

[14] Anderson, J.R., et al., "Results of an On-going Long Duration Ground Test of the DS1 Flight Spare Ion Engine," AIAA Paper 99-2857, June 1999.

[15] Kaufman, H.R., "Technology of Electron Bombardment Ion Thrusters," Advances in Electronics

and Electron Physics, vol. 36, Academic Press, Inc., New York, 1974, pp. 265-373.
[16] Patterson, M.J., "Low-Isp Derated Ion Thruster Operation," AIAA Paper 92-3203, July 1992.
[17] Soulas, G.C. and Rawlin, V.K., "Electron Backstreaming Limit Investigation," Internal Memorandum, NASA Glenn Research Center, April 1999.
[18] Aston, G. and Wilbur, P.J., "Ion Extraction from a Plasma," Journal of Applied Physics, vol. 52, no. 4, April 1981, pp. 2614-2626.
[19] Baragiola, R.A., et al., "Ion-Induced Electron Emission from Clean Metals," Surface Science, vol. 90, North-Holland Publishing Company, 1979, pp. 240-255.
[20] Patterson, M.J., Haag, T.W., and Hovan, S.A., "Performance of the NASA 30 cm Ion Thruster," IEPC Paper 93-108, September 1993.
[21] MacRae. G.S., Zavesky, R.J., and Gooder, S.T., "Structural and Thermal Response of 30 cm Diameter Ion Thruster optics," AIAA Paper 89-2719, July 1989.
[22] Rawlin, V.K., Personal Communication, June 2000.
[23] Kreiner, K., Personal Communication, July 2000.

Table 1. Nominal thruster operating parameters.

Input Power,[a] kW	Beam Current,[b] A	Beam Voltage,[b] V	Accelerator Voltage, V	Neutralizer Keeper Current, A	Main Flow, sccm	Discharge Cathode Flow, sccm	Neutralizer Flow, sccm
0.5[c]	0.51	650	-150	2.0	5.98	2.47	2.40
1.0[c]	0.71	1100	-150	2.0	8.30	2.47	2.40
1.4[c]	1.10	1100	-180	1.5	14.4	2.47	2.40
1.7[c]	1.30	1100	-180	1.5	17.2	2.56	2.49
1.8[c]	1.49	1100	-180	1.5	18.5	2.72	2.65
2.3[c]	1.76	1100	-180	1.5	23.4	3.70	3.60
3.0	1.76	1500	-250	1.5	23.1	3.54	3.60
4.6	2.70	1500	-250	1.5	36.3	3.54	4.80

[a]Nominal values.
[b]Power supply current or voltage.
[c]Nominal NSTAR operating condition.

Table 2. Perveance margins and electron backstreaming limit magnitudes for titanium and molybdenum optics.

Input Power, kW	Perveance Margin, V				Electron Backstreaming Limit Magnitude, V			
	Ti Set A[a] (ref. 6)	Ti Set A	Ti Set B	Mo	Ti Set A[a] (ref. 6)	Ti Set A	Ti Set B	Mo
0.5[b]	50	115	-	155	60	72	-	67
1.0[b]	410	470	510	520	111	125	127	123
1.4[b]	290	355	400	445	125	139	143	137
1.7[b]	245	285	345	395	138	148	149	143
1.8[b]	-	225	295	350	-	152	152	147
2.3[b]	110	155	235	275	143	159	160	154
3.0	-	635	-	-	-	201	-	-
4.6	-	380	-	-	-	222	-	-

[a]Data from ref. 6 with cold gap at active area mid-radius and center cold 23-38% larger than NSTAR design; engineering model NSTAR thruster used.
[b]Nominal NSTAR operating condition.

Table 3. Peak beam current densities and screen grid ion transparencies for titanium and molybdenum optics.

Input Power, kW	Peak Beam Current Densities,[a] mA/cm^2			Screen Grid Ion Transparency		
	Ti Set A	Ti Set B	Mo	Ti Set A	Ti Set B	Mo
0.5[b]	2.6	-	2.3	0.882	-	0.826
1.0[b]	3.5	3.6	3.1	0.914	0.882	0.876
1.4[b]	5.0	5.2	4.3	0.922	0.885	0.880
1.7[b]	5.6	5.8	4.9	0.921	0.876	0.875
1.8[b]	6.1	6.2	5.3	0.911	0.864	0.864
2.3[b]	6.7	6.9	6.1	0.900	0.843	0.851
3.0	7.0	-	-	0.928	-	-
4.6	9.0	-	-	0.897	-	-

[a]Peak beam current densities at 49 mm downstream of the geometric center of the optics; peak beam current densities occurred at approximately the radial center of the grid active area.
[b]Nominal NSTAR operating condition.

Table 4. Divergence half-angles at 90% of total beam current and beam divergence thrust correction factors for titanium and molybdenum optics.

Input Power, kW	Divergence Half-Angle at 90% of Beam Current, degrees		Thrust Correction Factor for Beam Divergence	
	Ti Set A	Mo	Ti Set A	Mo
0.5[b]	21	22	0.98	0.98
1.0[b]	22	-	0.97	-
1.4[b]	21	22	0.98	0.98
1.7[b]	20	-	0.98	-
1.8[b]	19	-	0.98	-
2.3[b]	19	19	0.98	0.97
3.0	23	23	0.97	0.98
4.6	20	-	0.98	-

[a]Peak beam current densities occurred at approximately the radial center of the grid active area.
[b]Nominal NSTAR operating condition.

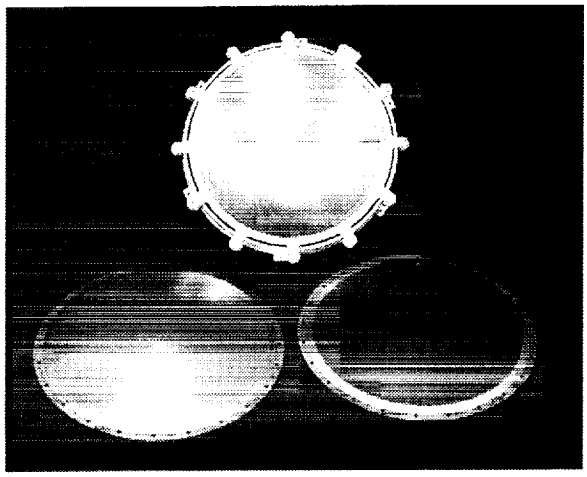

Fig. 1. Photograph of titanium grids with and without the thruster mounting ring.

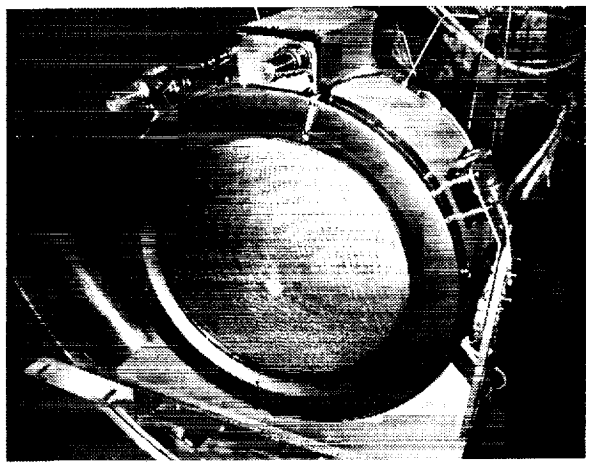

Fig. 2. Titanium optics installed onto a NASA 30 cm ion thruster.

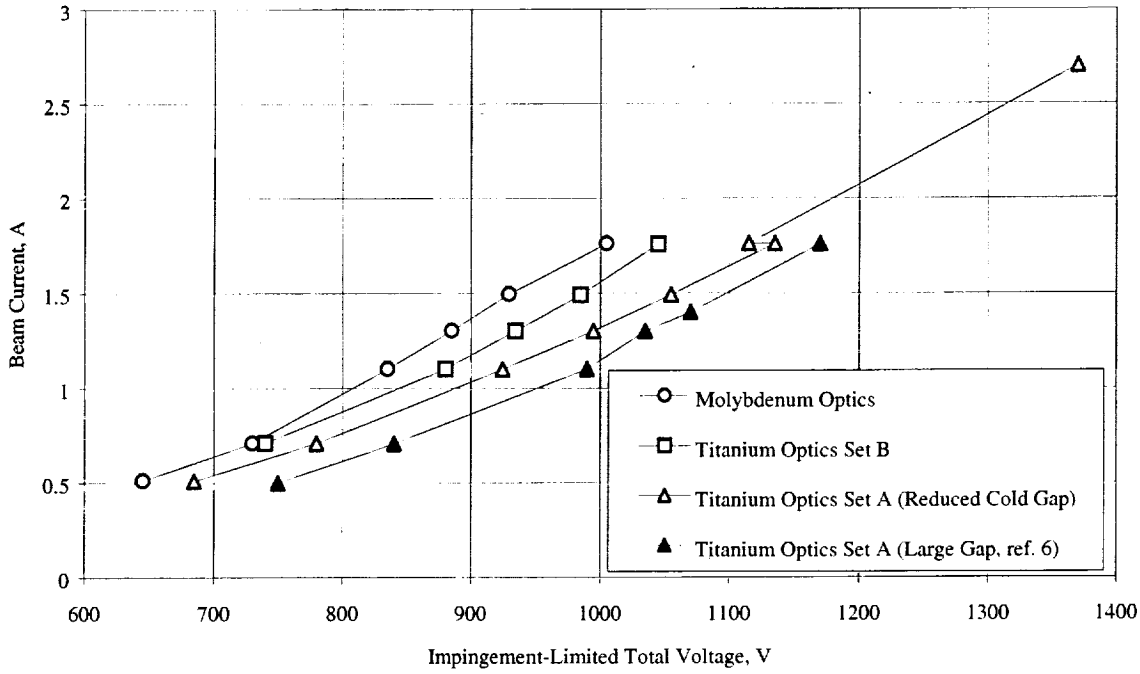

Fig. 3. Beam current as a function of impingement-limited total voltage for titanium and molybdenum optics.

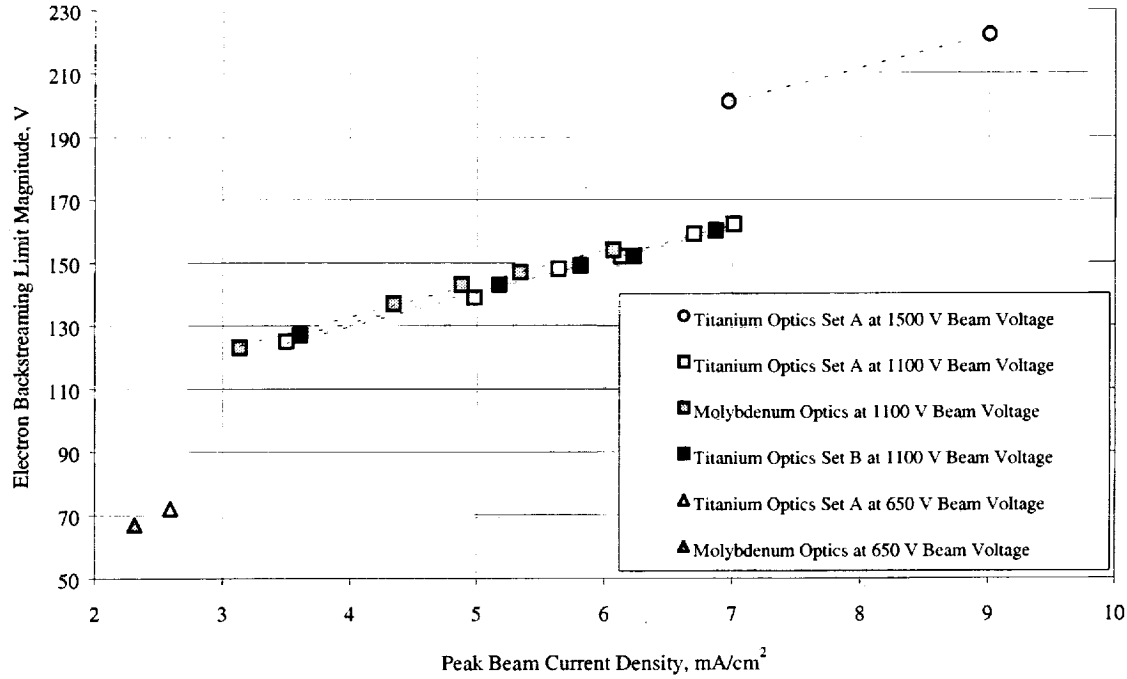

Fig. 4. Electron backstreaming limit as a function of peak beam current density for titanium and molybdenum optics. Peak beam current densities were measured 49 mm downstream of the optics' center.

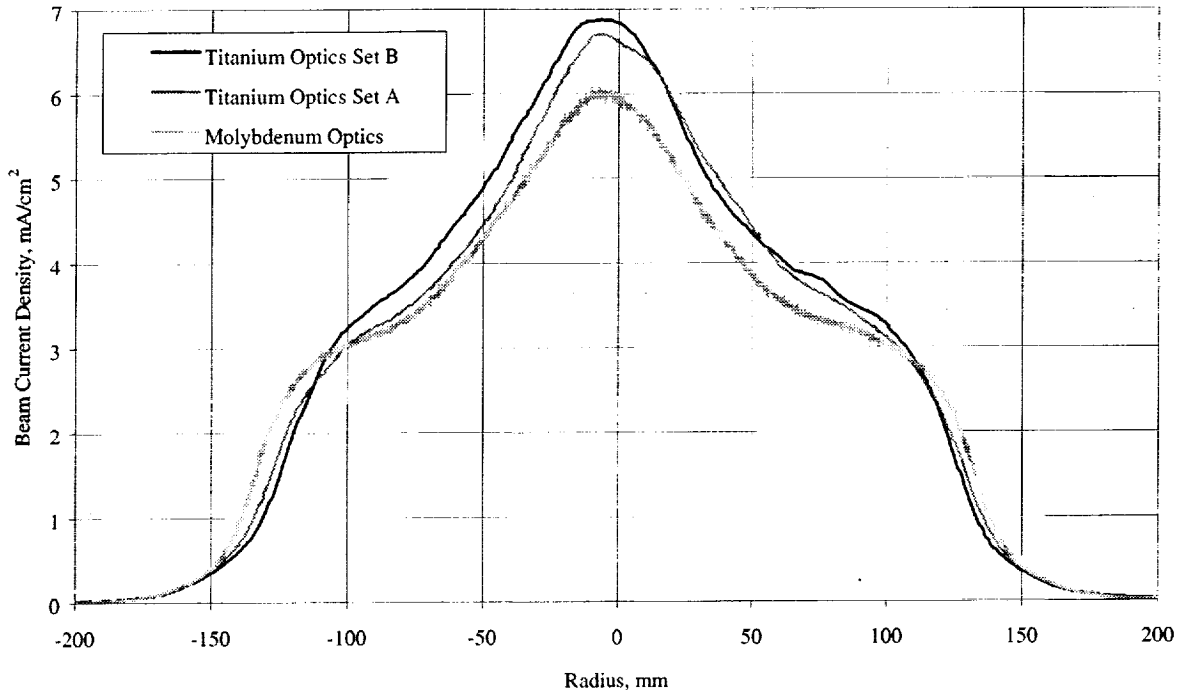

Fig. 5. Radial beam current density profiles for both titanium and molybdenum optics at a 1.76 A beam current and a 2.3 kW nominal input power.

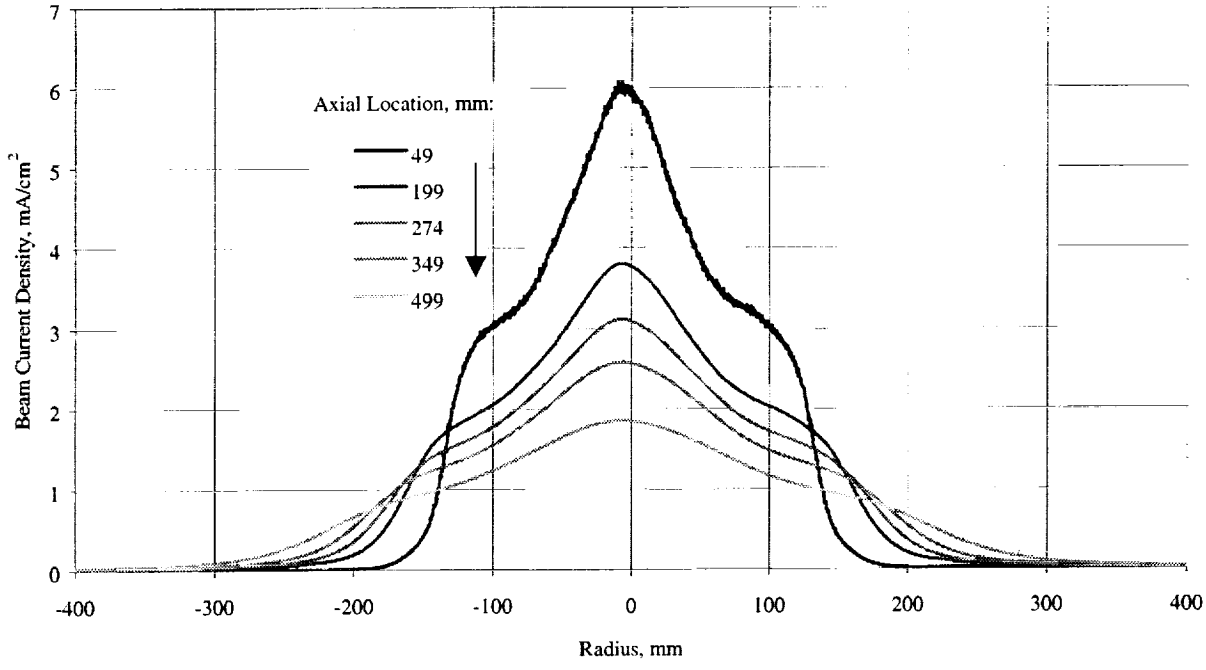

Fig. 6. Radial beam current density profiles at five axial locations for molybdenum optics at a 1.76 A beam current and a 2.3 kW nominal input power.

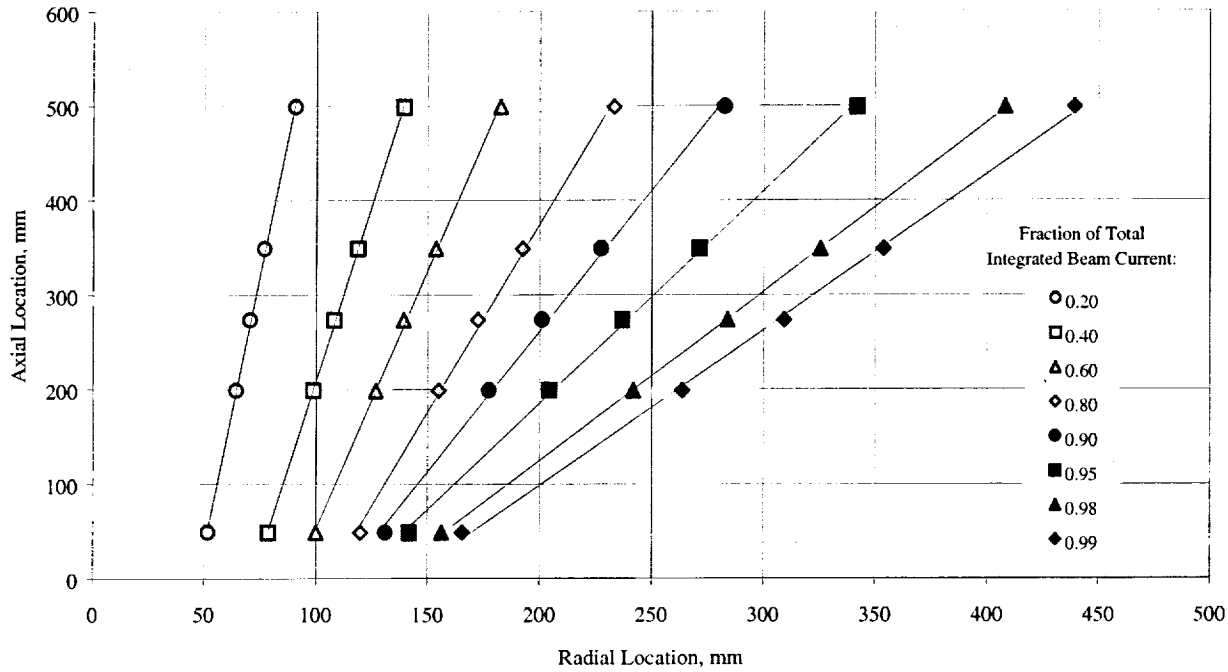

Fig. 7. Sample fractions of total integrated beam current for molybdenum optics at a 1.76 A beam current and a 2.3 kW nominal input power.

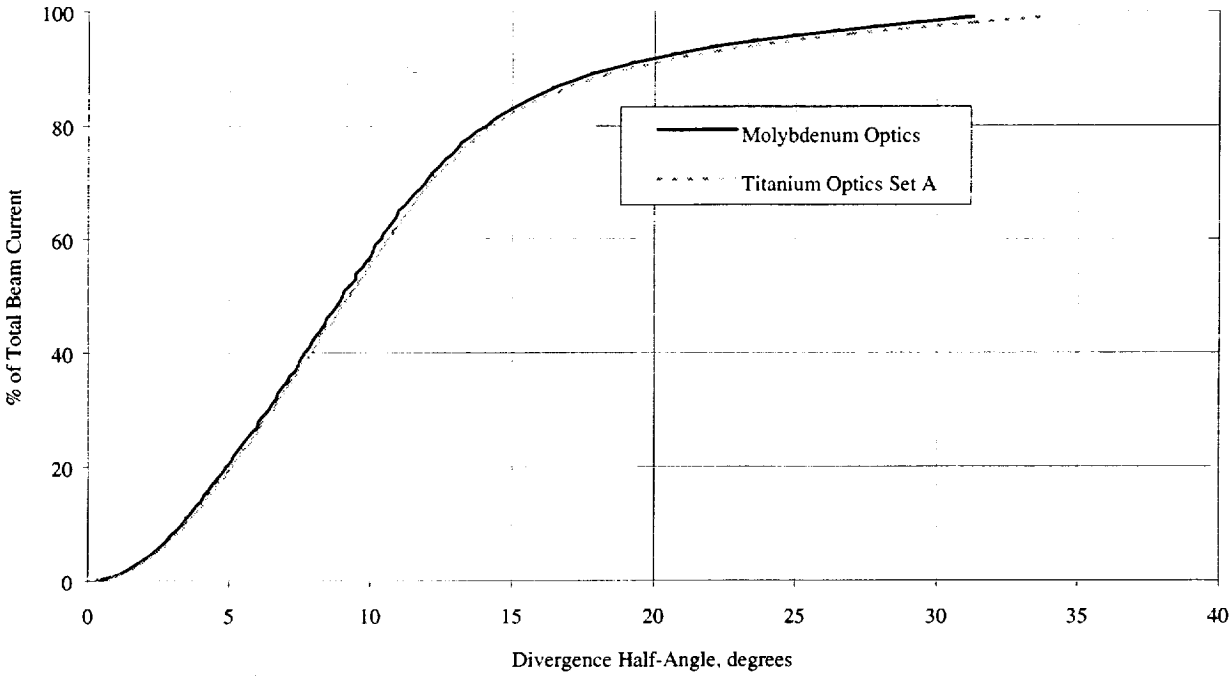

Fig. 8. Percentage of total beam current as a function of divergence half-angle for both titanium and molybdenum optics at a 1.76 A beam current and a 2.3 kW nominal input power.

REPORT DOCUMENTATION PAGE

Form Approved
OMB No. 0704-0188

1. AGENCY USE ONLY (*Leave blank*)	2. REPORT DATE	3. REPORT TYPE AND DATES COVERED
	November 2000	Technical Memorandum

4. TITLE AND SUBTITLE

Performance of Titanium Optics on a NASA 30 cm Ion Thruster

5. FUNDING NUMBERS

WU–632–6B–1B–00

6. AUTHOR(S)

George C. Soulas, John E. Foster, and Michael J. Patterson

7. PERFORMING ORGANIZATION NAME(S) AND ADDRESS(ES)

National Aeronautics and Space Administration
John H. Glenn Research Center at Lewis Field
Cleveland, Ohio 44135–3191

8. PERFORMING ORGANIZATION REPORT NUMBER

E–12485

9. SPONSORING/MONITORING AGENCY NAME(S) AND ADDRESS(ES)

National Aeronautics and Space Administration
Washington, DC 20546–0001

10. SPONSORING/MONITORING AGENCY REPORT NUMBER

NASA TM—2000-210518
AIAA–2000–3814

11. SUPPLEMENTARY NOTES

Prepared for the 36th Joint Propulsion Conference and Exhibit cosponsored by the AIAA, ASME, SAE, and ASEE, Huntsville, Alabama, July 17–19, 2000. Responsible person, George C. Soulas, organization code 5430, 216–977–7419.

12a. DISTRIBUTION/AVAILABILITY STATEMENT

Unclassified - Unlimited
Subject Category: 20 Distribution: Nonstandard

Available electronically at http://gltrs.grc.nasa.gov/GLTRS

This publication is available from the NASA Center for AeroSpace Information, 301–621–0390.

12b. DISTRIBUTION CODE

13. ABSTRACT ***(Maximum 200 words)***

The results of performance tests with two titanium optics sets are presented and compared to those of molybdenum optics. All tests were conducted on a 30 cm ion thruster that was nearly identical to the NSTAR thruster design. Optics performance tests were conducted over a thruster input power range of 0.5 to 4.6 kW. Optics performance including impingement-limited total voltages, electron backstreaming limits, screen grid ion transparencies, near-field beam current density profiles, beam divergence angles, and beam divergence thrust correction factors were determined throughout this power range. The impingement-limited total voltages for titanium optics were within 10 to 55 V of those for molybdenum optics. Electron backstreaming limit magnitude as a function of peak beam current density for both molybdenum and titanium optics were within a few volts of each other, indicating similar hot grid gaps for these two grid materials during steady-state operation. Beam divergence half-angles at 90 percent of the total beam current and thrust correction factors for both titanium optics sets were within 1° and 1 percent, respectively, of those for molybdenum optics. When thruster power was increased to 2.3 kW immediately following discharge ignition, the titanium screen grid came into contact with the accelerator grid within 5 min of ignition. Relative to molybdenum, titanium's larger thermal expansion and smaller thermal conductivity likely caused the screen grid to thermally expand more relative to the accelerator grid during startup.

14. SUBJECT TERMS

Ion thruster; Ion optics; Grids

15. NUMBER OF PAGES

19

16. PRICE CODE

A03

17. SECURITY CLASSIFICATION OF REPORT	18. SECURITY CLASSIFICATION OF THIS PAGE	19. SECURITY CLASSIFICATION OF ABSTRACT	20. LIMITATION OF ABSTRACT
Unclassified	Unclassified	Unclassified	